Science Translational Medicine
AAAS

stm.sciencemag.org/cgi/content/full/12/537/eaaw0262/DC1

Supplementary Materials for

Urinary detection of lung cancer in mice via noninvasive pulmonary protease profiling

Jesse D. Kirkpatrick, Andrew D. Warren, Ava P. Soleimany, Peter M. K. Westcott, Justin C. Voog, Carmen Martin-Alonso, Heather E. Fleming, Tuomas Tammela, Tyler Jacks, Sangeeta N. Bhatia*

*Corresponding author. Email: sbhatia@mit.edu

Published 1 April 2020, *Sci. Transl. Med.* **12**, eaaw0262 (2020)
DOI: 10.1126/scitranslmed.aaw0262

The PDF file includes:

Other Supplementary Material for this manuscript includes the following:

(available at stm.sciencemag.org/cgi/content/full/12/537/eaaw0262/DC1)

Data file S1 (Microsoft Excel format). Raw data from figures.

Methods

Gene expression analysis

Human RNA-Seq data from The Cancer Genome Atlas (TCGA) Research Network *(28)* was downloaded from https://www.cancer.gov/tcga and human RNA-Seq data from the Lung Genomics Research Consortium (LGRC) *(31)* was downloaded from https://www.lung-genomics.org/research. The list of human extracellular protease genes was obtained from UniProt. Differential expression analysis on the TCGA data was performed using the DESeq2 differential expression library in the R statistical environment (Fig. 2C) *(29, 43)*. AUROC analysis was performed for the TCGA and LGRC datasets using FPKM values from disease samples (LUAD, ILD, and COPD) and their respective controls (NAT for LUAD, normal lung for ILD and COPD), using GraphPad Prism version 7.0a (fig. S2). Genes in the LGRC dataset for which at least half of the samples had FPKM values greater than zero were included in the AUROC analysis, but all zero values were excluded. FPKM values for the KP model *(25)* were downloaded from Gene Expression Omnibus (GEO; GSE84447). Top 20 extracellular endoproteases were identified by averaging FPKM values across all tumor bearing mice and dividing by the average FPKM values for normal mice (Fig. 2A). Genes for which neither of the two normal lung samples had nonzero FPKM values were excluded. Microarray counts for the K dataset *(26)* were downloaded from GEO (GSE49200). Gene expression fold changes were determined by performing quantitative significance analysis of microarrays (SAM) using the "Standard" regression method, 100 permutations, and 10 neighbors for k-nearest neighbors (KNN) classification (Fig. 2B) *(27)*.

Pre-ranked GSEA was performed on the LUAD and LUSC gene expression datasets from TCGA using a gene set containing the top 20 overexpressed proteases in the KP model (Fig. 2D)

or the 15 genes of the LUAD protease panel (fig. S3) *(25)*. The pre-ranked list of $\log_2$(Fold Change) was generated previously by DESeq2. A minimum of 10000 permutations by gene set were performed to calculate the *P* value. GSEA was performed via the GenePattern online software *(44)* and the GSEA desktop application using the "classic" scoring scheme.

Fluorogenic substrate characterization

Fluorogenic protease substrates were synthesized by CPC Scientific. Recombinant proteases were purchased from Enzo Life Sciences, R&D Systems, and Haematologic Technologies. For recombinant protease assays, fluorogenic substrates PPQ1-14 (1 μM final concentration) were incubated in 30 μL final volume in appropriate enzyme buffer, according to manufacturer specifications, with 12.5 nM recombinant enzyme at 37°C (Fig. 3). Proteolytic cleavage of substrates was quantified by increases in fluorescence over time by fluorimeter (Tecan Infinite M200 Pro). Enzyme cleavage rates were quantified as relative fluorescence increase over time normalized to fluorescence before addition of protease. Hierarchical clustering was performed in GENE-E (https://software.broadinstitute.org/GENE-E/, Broad Institute), using fluorescence fold changes at 45 minutes.

Intratracheal instillation and in vivo aerosolization studies

For all mouse experiments, anesthesia was induced by isoflurane inhalation (Zoetis), and mice were monitored during recovery. For intratracheal instillation studies, a volume of 50 μl was administered by passive inhalation following intratracheal intubation with a 22G flexible plastic catheter (Exel), as described elsewhere *(24)*. All aerosolization experiments used a MicroSprayer Aerosolizer – Model MSA-250-M (Penn-Century. Inc.) with a volume of 50 μl/mouse by placing the aerosolizer tip in the trachea immediately proximal to the carina and rapidly depressing the plunger.

Biodistribution studies

Biodistribution studies were performed in healthy male C57BL/6 mice. VT750-NHS Ester (PerkinElmer) was coupled to 8-arm 40 kDa PEG-amine (PEG-8_{40kDa}-amine, JenKem) at a 4:1 molar ratio, reacted overnight, and purified by spin filtration (Amicon Ultra centrifugal filter units, Sigma). Mice were lightly anesthetized via isoflurane inhalation, and PEG-8_{40kDa}-VT750 (50 μl volume, 5 μM concentration by VT750 absorbance) was administered by intratracheal instillation (Fig. 4B-C) or aerosolization (fig. S8A-B). Mice in the IV cohort were intravenously administered an equal dose of PEG-8_{40kDa}-VT750. Animals were sacrificed by CO_2 asphyxiation at the indicated timepoints post-inhalation/injection and organs were removed for imaging (LICOR Odyssey). Organ fluorescence was quantified in Fiji *(45)* by manually outlining organs, using the "Measure" feature, and taking the mean intensity.

Blood for pharmacokinetics measurements was collected using retro-orbital bleeds with 15 μL glass capillary collection tubes. Blood was diluted in 40 μL phosphate buffered saline (PBS) with 5 mM ethylenediaminetetraacetic acid (EDTA) to prevent clotting, centrifuged for 5 min at 5,000 x g, and fluorescent reporter concentration was quantified in 384-well plates relative to standards (LICOR Odyssey) (fig. S9C).

For immunohistochemical visualization of nanoparticles following IT administration, EZ-Link NHS-Biotin (Thermo Scientific) was coupled to PEG-8_{40kDa}-amine at a 2:1 molar ratio and reacted overnight, followed by spin filtration (Amicon Ultra centrifugal filter units, Sigma). Pulmonary delivery of PEG-8_{40kDa}-biotin (50 μl volume, 10 μM concentration) was performed by intratracheal instillation (Fig. 4D-E) or aerosolization (fig. S8C-F). Fixation was performed 10-30 minutes later by inflating lungs with 10% formalin. Lungs were excised, fixed in 10% formalin at 4°C overnight, and embedded in paraffin blocks. 5 μm tissue slices were stained for biotin using the streptavidin-HRP ABC kit (Vector Labs) with 3,3′-Diaminobenzidine (DAB).

Slides were scanned using the 20x objective of the Pannoramic 250 Flash III whole slide scanner (3DHistech).

In vitro aerosolization studies

Analysis of nanoparticle stability and protease cleavage susceptibility following aerosolization used 0.1 μm-filtered 250 μM PEG-8_{40kDa} scaffold (fig. S7B-E) or 5 μM PPQ5 PEG-8_{40kDa} nanosensors (fig. S7F). Protease cleavage assays of aerosolized nanoparticles used 50 nM of recombinant human MMP13 (Enzo).

Toxicity studies

Activity-based nanosensor constructs (GluFib-Substrate-PEG-8_{40kDa}) were synthesized by CPC Scientific. Activity-based nanosensors were dosed (50 μL total volume, 20 μM concentration per nanosensor in mannitol buffer (0.28 M mannitol, 5 mM sodium phosphate monobasic, 15 mM sodium phosphate dibasic, pH 7.0-7.5)) by intratracheal instillation into healthy male C57BL/6 mice. The mass of each mouse was monitored for 11 days post-administration and compared with masses of control mice administered mannitol buffer. Heart, lung, liver, spleen, and kidney tissues were collected from the mice at 2 h, 24 h, or 11 days post-administration, fixed in 10% formalin, paraffin embedded, stained with haematoxylin and eosin, and then examined by a veterinary pathologist (Dr. Roderick Bronson).

Clearance studies

VT750-NHS Ester (PerkinElmer) was coupled to 8-arm 40 kDa PEG-amine (PEG-8_{40kDa}-amine, JenKem) at a 4:1 molar ratio, reacted overnight, and purified by spin filtration (Amicon Ultra centrifugal filter units, Sigma). Mice were lightly anesthetized via isoflurane inhalation, and PEG-8_{40kDa}-VT750 (50 μl volume, 20 μM concentration by VT750 absorbance) was administered by intratracheal instillation (fig. S5). Animals were sacrificed by CO_2 asphyxiation at the indicated timepoints and organs were removed for imaging (LICOR Odyssey). Organ

fluorescence was quantified in Fiji *(45)* by manually outlining organs, using the "Measure" feature, and taking the mean intensity. Kinetic data was fit using nonlinear regression in GraphPad 8.0 (Prism). Lung data was fit to an exponential decay model ($Y=Y_0e^{(-Kt)}$; Y, fluorescence; Y_0, initial fluorescence; K, rate constant; t, time), and all other organ data was fit to a two-phase growth and decay model ($Y=A1e^{(-t/B1)}+A2e^{(-t/B2)}$; Y, fluorescence; t, time; A1/A2/B1/B2, constants).

KP lung adenocarcinoma model

KP tumors were initiated by intratracheal administration of 50 μL of adenovirus-SPC-Cre (2.5×10^8 plaque-forming units (PFU) in Opti-MEM with 10 mM calcium chloride ($CaCl_2$)) in male B6/SV129 $Kras^{LSL\text{-}G12D/+}$; $Trp53^{fl/fl}$ (KP) mice (between 18 and 30 weeks old) under isoflurane anesthesia *(24)*. Control cohorts consisted of age and sex-matched mice that did not undergo intratracheal administration of adenovirus. Tumor growth was monitored by microCT imaging (General Electric) and was scored by a blinded radiation oncologist (Dr. Justin Voog) (table S2) using MicroView (Parallax Innovations). Tumor volumes were calculated by using the ROI sphere/elliptical tool. Tumor-bearing mice and age-matched controls were administered activity-based nanosensor constructs via intratracheal intubation at 5, 7.5, and 10.5 weeks after tumor induction.

EA lung adenocarcinoma model

Tumors were initiated in male C57BL/6 mice between 6 and 10 weeks old as described previously *(34)*, by intratracheal administration of 50 μL adenovirus expressing the Ad-EA vector (Viraquest, 1.5 x 10^8 PFU in Opti-MEM with 10 mM $CaCl_2$). Control cohorts consisted of age and sex-matched mice that did not undergo intratracheal administration of adenovirus. Tumor-bearing mice and age-matched controls were administered activity-based nanosensor constructs via intratracheal intubation at 5, 7.5, and 10.5 weeks after tumor induction.

Colorectal cancer xenograft model

For xenograft studies, LS174T (ATCC CL-188) cells were cultured in Eagle's Minimal Essential Medium (EMEM, ATCC) supplemented with 10% (v/v) FBS (Gibco) and 1% (v/v) penicillin-streptomycin (CellGro). Cells were passaged and harvested for inoculation when confluence reached 80%. Female NCR nude mice (4-5 weeks, Taconic) were injected bilaterally with 3 x 10^6 LS174T cells, resuspended in Opti-MEM (ThermoFisher), per flank. Ten days after inoculation, tumor-bearing mice and age-matched controls were administered activity-based nanosensor constructs via intratracheal intubation.

Lipopolysaccharide (LPS) model

Lung inflammation was induced in 18 to 20 week-old male C57BL/6 mice via intratracheal administration of 0.3 mg of LPS (Sigma Aldrich) in 50 μl water, under isoflurane anesthesia. LPS-treated mice and age and sex-matched healthy controls were administered activity-based nanosensors 3 days after LPS induction.

In vivo characterization of activity-based nanosensors

All activity-based nanosensor experiments were performed in the morning and in accordance with institutional guidelines. Nanosensors (GluFib-Substrate-PEG-8_{40kDa}) for urinary experiments were synthesized by CPC Scientific. Nanosensors were dosed (50 μL total volume, 20 μM concentration per nanosensor) in mannitol buffer (0.28 M mannitol, 5 mM sodium

phosphate monobasic, 15 mM sodium phosphate dibasic, pH 7.0-7.5) by intratracheal intubation, as described above, immediately followed by a subcutaneous injection of PBS (200 µl) to increase urine production. Bladders were voided 60 minutes after nanosensor administration, and all urine produced 60-120 min after administration was collected using custom tubes in which the animals rest upon 96-well plates that capture urine. Urine was pooled and frozen at -80°C until analysis by LC-MS/MS.

LC-MS/MS reporter quantification

LC-MS/MS was performed by Syneos Health using a Sciex 6500 triple quadrupole instrument. Briefly, urine samples were treated with ultraviolet (UV) irradiation to photocleave the 3-Amino-3-(2-nitro-phenyl)propionic Acid (ANP) linker and liberate the Glu-Fib reporter from residual peptide fragments. Samples were extracted by solid-phase extraction and analyzed by multiple reaction monitoring by LC-MS/MS to quantify concentration of each Glu-Fib mass variant. Analyte quantities were normalized to a spiked-in internal standard and concentrations were calculated from a standard curve using PAR to the internal standard. Mean normalization was performed on PAR values to account for mouse-to-mouse differences in activity-based nanosensor inhalation efficiency and urine concentration.

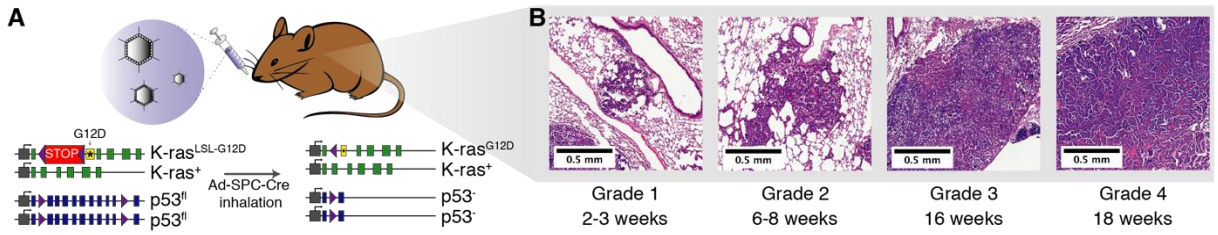

Fig. S1. KP model genetically and histologically recapitulates human LUAD. (**A**) Disease was induced in the KP model by intratracheal instillation of adenovirus expressing Cre recombinase under the control of the surfactant protein C (SPC) promoter, which resulted in activation of mutant *K-ras*^{G12D} and excision of both copies of *Trp53* in type II alveolar cells *(24)*. (**B**) Histologically, disease progressed from low grade dysplasia to invasive adenocarcinoma over 18-20 weeks (shown are representative lesions of each grade in a single, advanced-stage KP mouse).

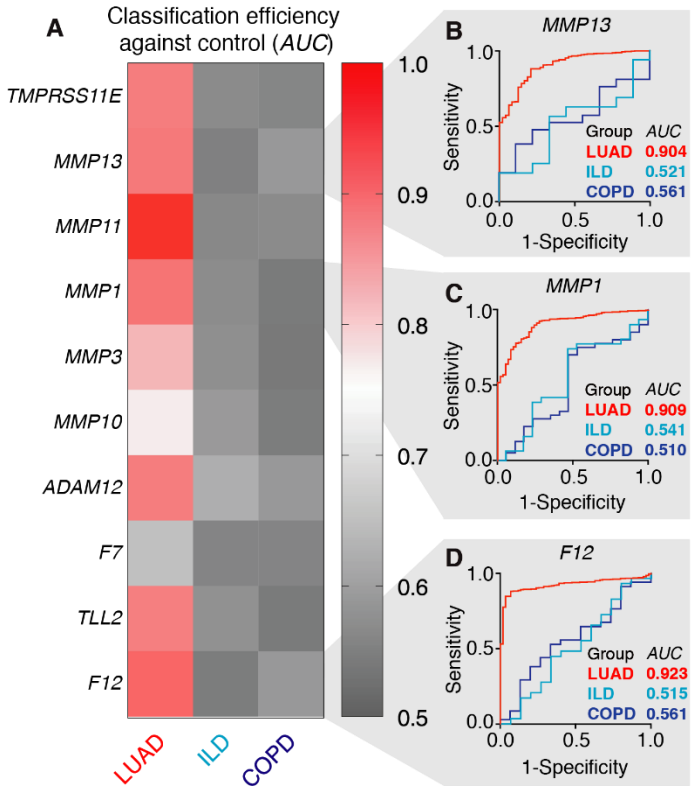

Fig. S2. Human LUAD-associated proteases are not overexpressed in benign lung diseases. (**A**) RNA-Seq data curated by the Lung Genomics Research Consortium (LGRC) was analyzed to assess the classification performance of human lung cancer-associated proteases in interstitial lung disease (ILD, *n* = 31) and chronic obstructive pulmonary disease (COPD, *n* = 41) against normal lung (*n* = 17). Of the top 20 overexpressed proteases in human LUAD, 10 were included in the LGRC dataset with FPKM values greater than zero for at least half of the samples. ROC analysis was performed for LUAD (from TCGA) and ILD and COPD (from LGRC) against their respective controls, using FPKM values for each protease. (**B-D**) ROC curves for individual proteases in the panel are shown.

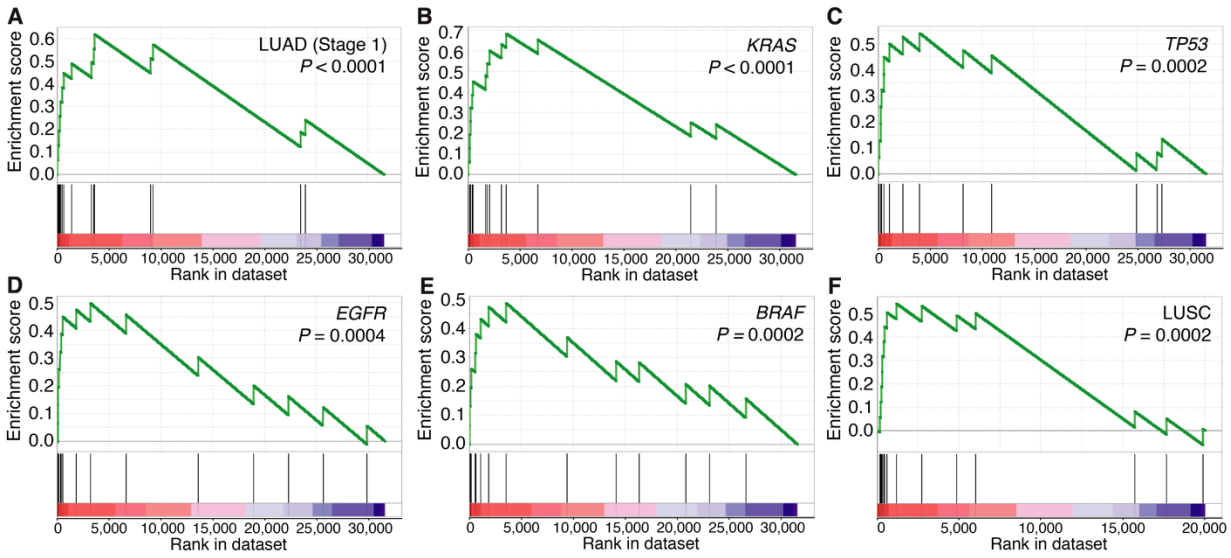

Fig. S3. LUAD protease panel genes are enriched across genetic and histological lung cancer subtypes. (**A-F**) GSEA plots showing enrichment of LUAD protease panel genes in stage I LUAD (A; n_{LUAD} = 302, n_{NAT} = 29; P < 0.0001), *KRAS*-mutant LUAD (B; n_{LUAD} = 75, n_{NAT} = 58; P < 0.0001), *TP53*-mutant LUAD (C; n_{LUAD} = 64, n_{NAT} = 58; P = 0.0002), *EGFR*-mutant LUAD (D; n_{LUAD} = 28, n_{NAT} = 58; P = 0.0004), *BRAF*-mutant LUAD (E; n_{LUAD} = 17, n_{NAT} = 58; P = 0.0002) and LUSC (F; n_{LUSC} = 233, n_{NAT} = 17; P = 0.0002).

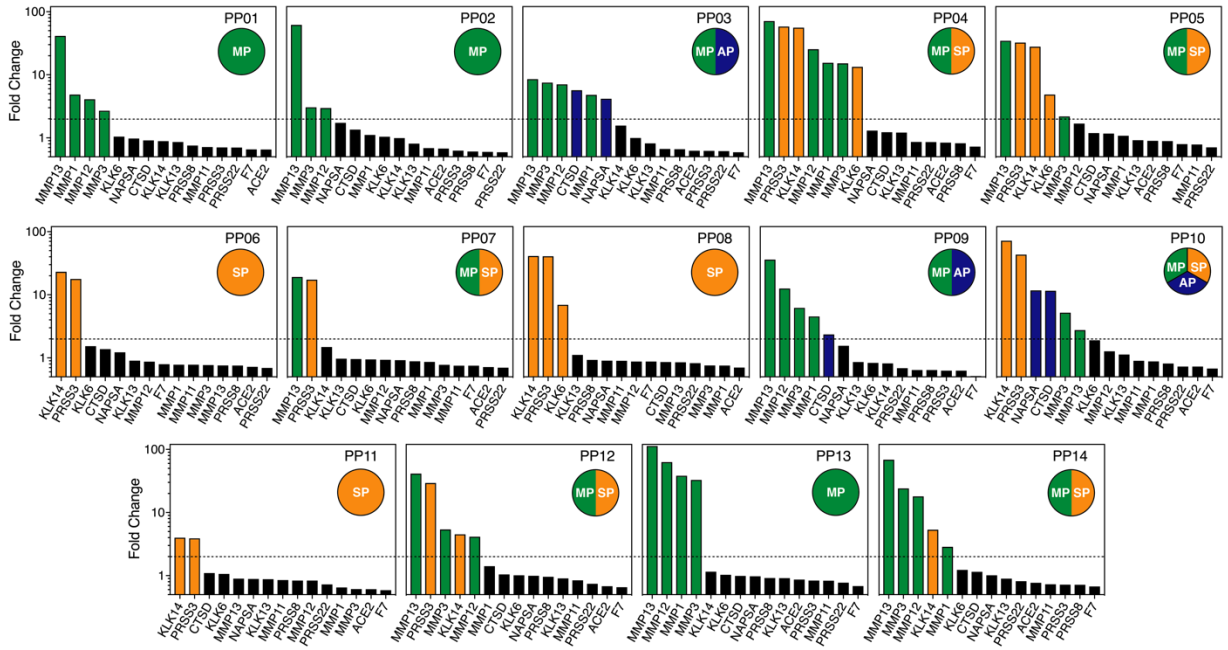

Fig. S4. Peptide substrates are cleaved by one or a combination of metalloproteases, serine proteases, and aspartic proteases. Quantification of *in vitro* proteolytic cleavage of fluorogenic peptide substrates. Y axis represents fluorescence fold change after 45 minutes of incubation with recombinant protease and dotted line is at fold change = 2. Bars are colored according to the catalytic class of the protease (green, metalloprotease-specific; orange, serine protease-specific; blue, aspartic protease-specific).

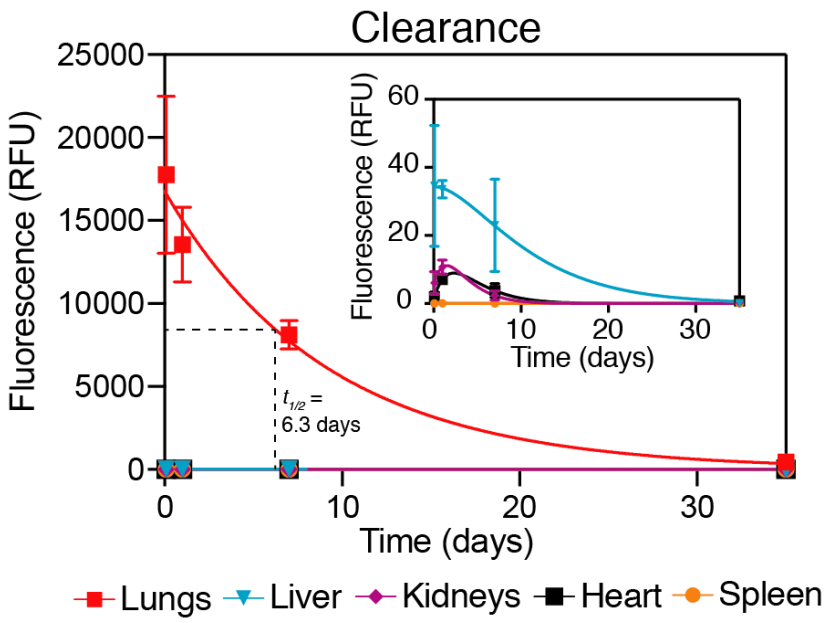

Fig. S5. Clearance of PEG-8_{40kDa} nanoparticles from lungs follows single-phase exponential decay kinetics. Fluorescence of lungs, liver, kidneys, heart, and spleen of mice after intrapulmonary delivery of VT750-labeled PEG-8_{40kDa} (n = 5 per time point). Points are mean +/- SD. Lung clearance data was fit with nonlinear regression using single phase exponential decay ($t_{1/2}$ = 6.3 days, R^2 = 0.86). Inset: liver, kidneys, heart, and spleen fluorescence are presented on a smaller scale y-axis and were fit with nonlinear regression using two phase exponential growth and decay.

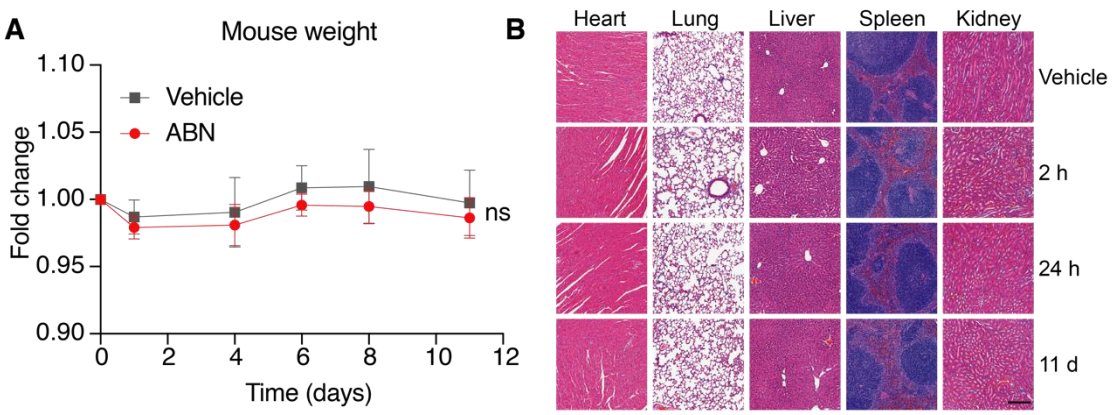

Fig. S6. No toxicity is observed in mice treated with intrapulmonary activity-based nanosensors. (**A**) Fold changes in mouse weights after treatment with either peptide-functionalized activity-based nanosensors (red; n = 9, days 0 to 1; n = 6, days 4 to 11) or mannitol buffer ('Vehicle'; grey; n = 8). (**B**) Representative H&E images of mouse organs at 2 hours, 1 day, and 11 days after intrapulmonary activity-based nanosensor treatment. Scale bar is 200 μm.

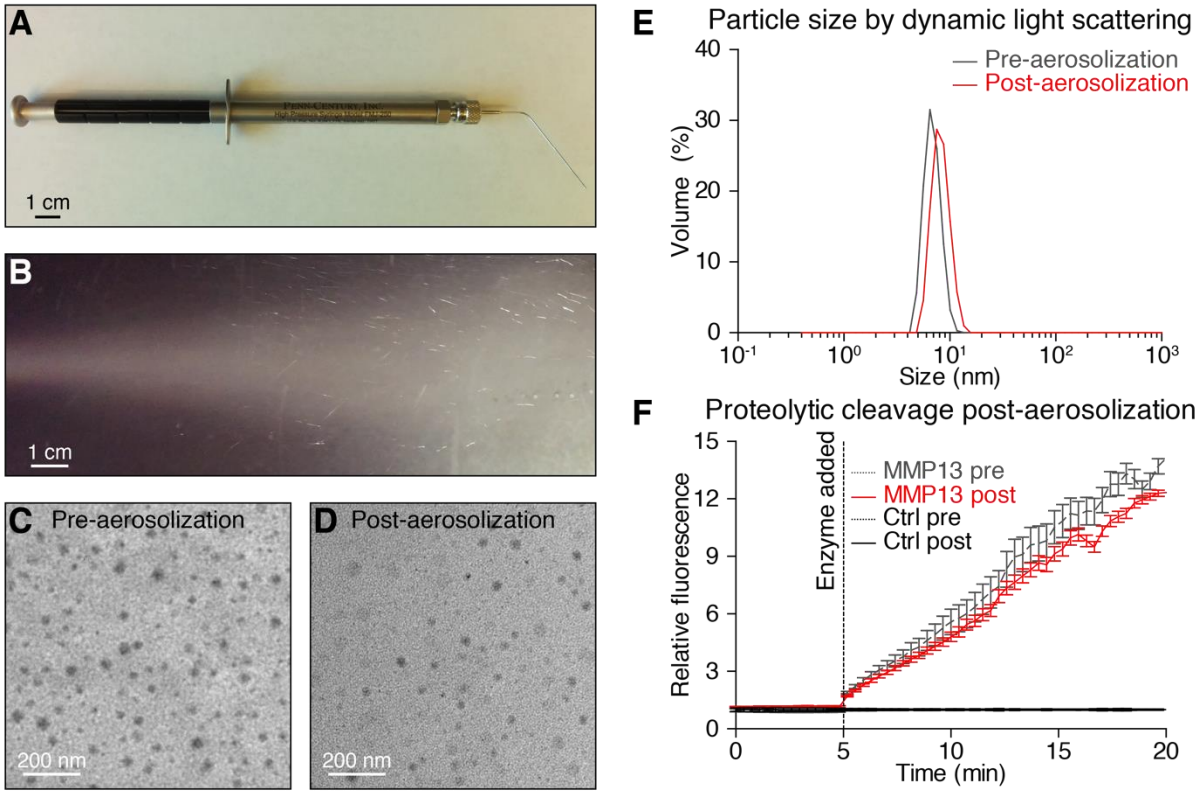

Fig. S7. Activity-based nanosensors are stable to aerosolization. (**A**) Device used for intratracheal administration of aerosolized nanosensors. (**B**) Aerosol produced from 50 µL of buffer. Scale for A and B is 1 cm. (**C, D**) TEM images of nanoparticle PEG-8_{40kDa} scaffold pre- (C) and post- (D) aerosolization. Scale is 200 nm. (**E**) Representative DLS quantification of particle sizes pre- and post-aerosolization of PEG-8_{40kDa} scaffold (n = 3). (**F**) Fluorescent dequenching by MMP13 of fluorogenic nanosensor PEG-PPQ5, pre (grey) (n = 4) and post (red) (n = 4) aerosolization. PEG-PPQ5 fluorescence change without addition of MMP13 is shown in black (n = 4).

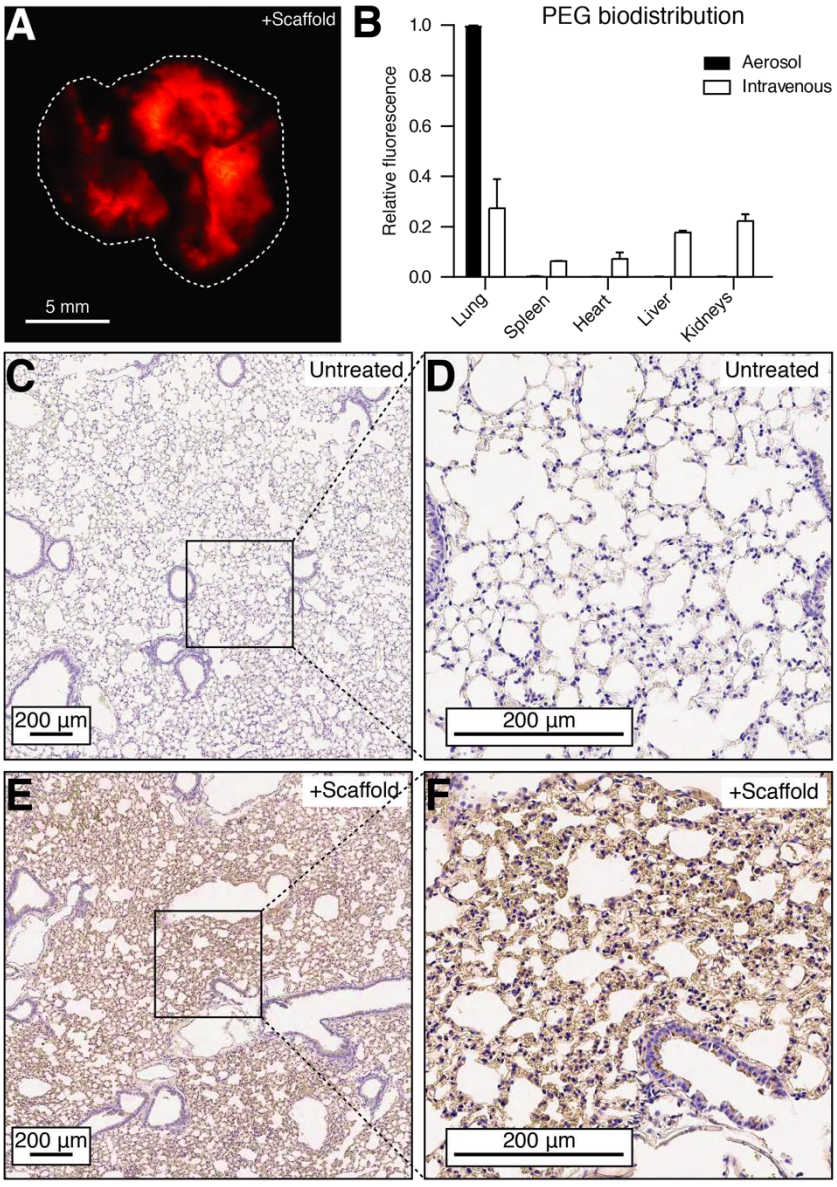

Fig. S8. Aerosolized nanoparticles penetrate deep within the lung and avoid distribution to off-target organs. (**A**) Representative image of lungs from a mouse treated with aerosolized fluorophore-labeled PEG-8_{40kDa}. Scale is 5 mm. (**B**) Organ-specific biodistribution of fluorophore-labeled PEG-8_{40kDa} 60 minutes after aerosol (red) (n = 2) or intravenous (grey) (n = 2) delivery. Error bars represent SEM. (**C-F**) Stained sections of untreated lungs (C-D) or lungs fixed 10 min post-aerosol delivery of biotin labeled PEG-8_{40kDa} (E-F). Scale bar for (C-F) is 200 µm.

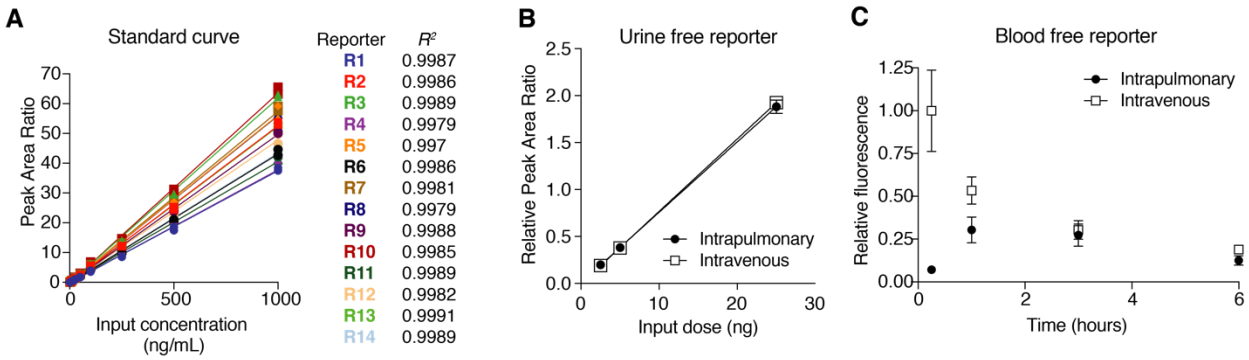

Fig. S9. Free reporters enter the bloodstream after pulmonary delivery and are detectable in the urine by mass spectrometry. (**A**) Glu-fib reporters were spiked into urine at concentrations ranging from 1 to 1000 ng/ml and LC-MS/MS was performed. Goodness of fit was assessed by linear regression and is given as Pearson's R^2. (**B**) Healthy mice (n = 4 each group) were administered MS-encoded free reporters (IT and IV) at doses ranging from 2.5 ng to 25 ng and urinary concentrations at 1 hour were assessed by LC-MS/MS ($slope_{IT}$ = 0.075 ng^{-1}, $slope_{IV}$ = 0.077 ng^{-1}). Geometric mean normalized peak area ratio is shown. Error bars represent SD. (**C**) Cy7-labeled free reporters were administered IT and IV and concentration in the blood was assessed over the following 6 hours (n = 4 each group). Error bars represent SD.

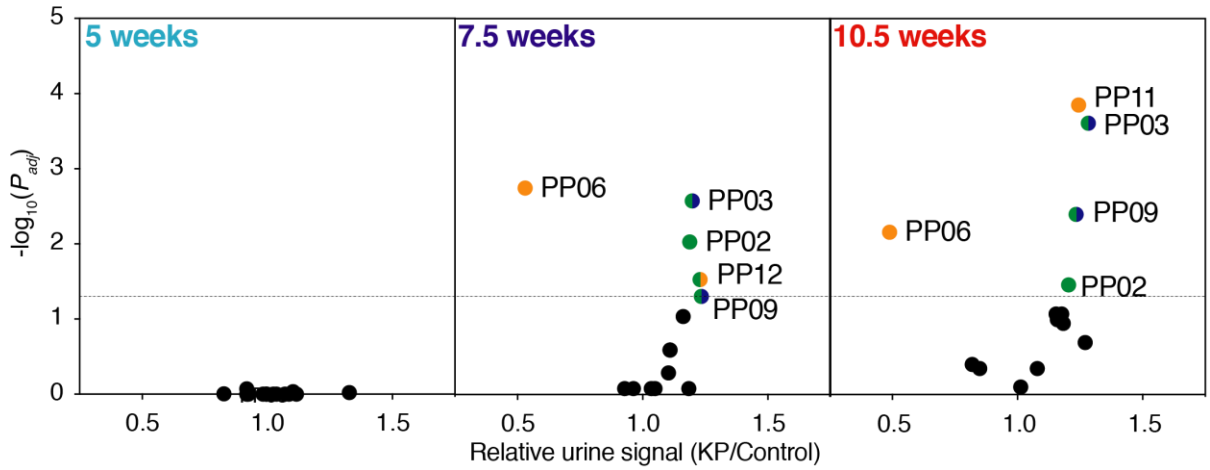

Fig. S10. Multiple reporters are differentially enriched in the urine of healthy mice and KP mice at 7.5 and 10.5 weeks. Mean normalized urinary reporter concentrations in KP mice and healthy mice were compared at 5 weeks (KP: n = 11; Control: n = 9), 7.5 weeks (KP: n = 11; Control: n = 12), and 10.5 weeks (KP: n = 12; Control: n = 12) after tumor induction and $-\log_{10}(P_{adj})$ was plotted against fold change between KP and control. Significance was calculated by two-tailed t-test followed by adjustment for multiple hypotheses with Holm-Sidak correction (for normally distributed reporters) or Mann-Whitney test with Bonferroni correction (for non-normal reporters PP12 and PP13 at 5 weeks; PP08 and PP09 at 7.5 weeks; PP01, PP04, and PP06 at 10.5 weeks). Dotted line is at P_{adj} = 0.05. Significant reporters are color-coded according to the classes of protease that cleave their corresponding peptide substrates *in vitro* (fig. S4) (green, metalloprotease-specific; orange, serine protease-specific; blue, aspartic protease-specific).

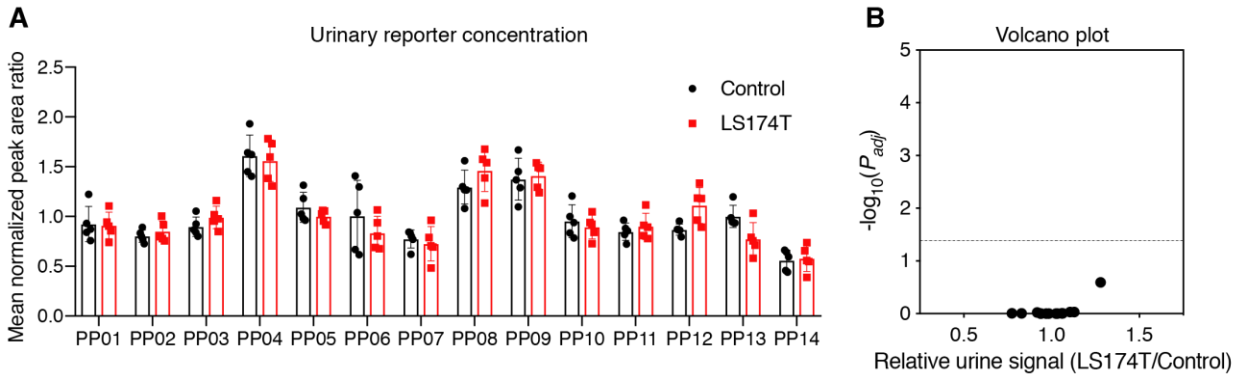

Fig. S11. Extrapulmonary disease is undetectable by intrapulmonary activity-based nanosensors. (A) Mean normalized urinary reporter output for healthy control mice (black, n = 5) or mice bearing flank LS174T tumors (red, n = 5). Error bars represent SD. **(B)** Volcano plot shows no differential enrichment of any of the 14 reporters detected in the urine of diseased mice relative to healthy controls, as assessed by two-tailed t-test followed by adjustment for multiple hypotheses with Holm-Sidak correction (for normally distributed reporters) or Mann-Whitney test with Bonferroni correction (for PP13).

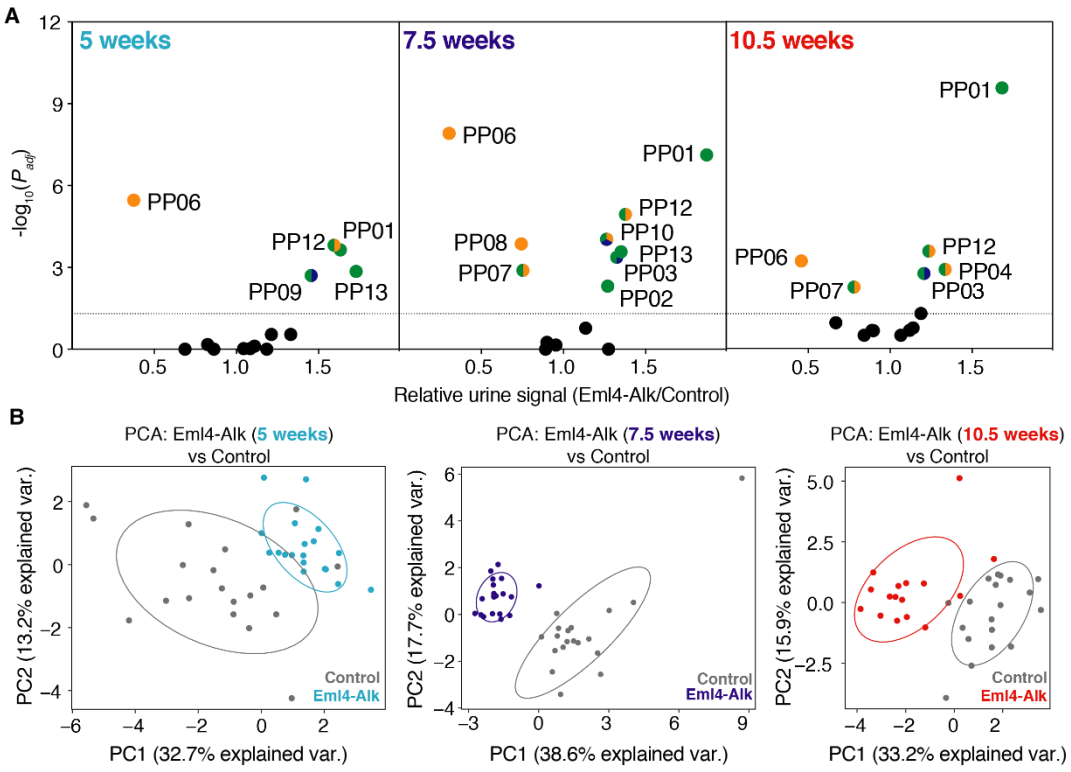

Fig. S12. Intrapulmonary activity-based nanosensors differentiate mice bearing Alk-driven lung cancer from healthy controls. (**A**) Mean normalized urinary reporter concentrations in EA mice and healthy mice were compared at 5 weeks (n = 19 each group) (left), 7.5 weeks (EA, n = 20; Control, n = 19) (middle) and 10.5 weeks (EA, n = 16; Control, n = 19) (right) after tumor induction and $-\log_{10}(P_{adj})$ was plotted against fold change between EA and control. Significance was calculated by two-tailed t-test with Holm-Sidak correction (for normally distributed reporters) or Mann-Whitney test with Bonferroni correction (for PP02, PP04, PP08, PP09, and PP12 at 5 weeks; PP04, PP06, PP08, PP13, and PP14 at 7.5 weeks; PP04, PP06, and PP14 at 10.5 weeks). Dotted line is at P_{adj} = 0.05. Significant reporters are color-coded according to the classes of protease that cleave their corresponding peptide substrates *in vitro* (fig. S4) (green, metalloprotease-specific; orange, serine protease-specific; blue, aspartic protease-specific). (**B**) PCA of urinary reporter output of EA mice and healthy controls at 5 weeks (n = 19 each group)

(left), 7.5 weeks (EA, *n* = 20; Control, *n* = 19) (middle) and 10.5 weeks (EA, *n* = 16; Control, *n* = 19) (right) after tumor induction.

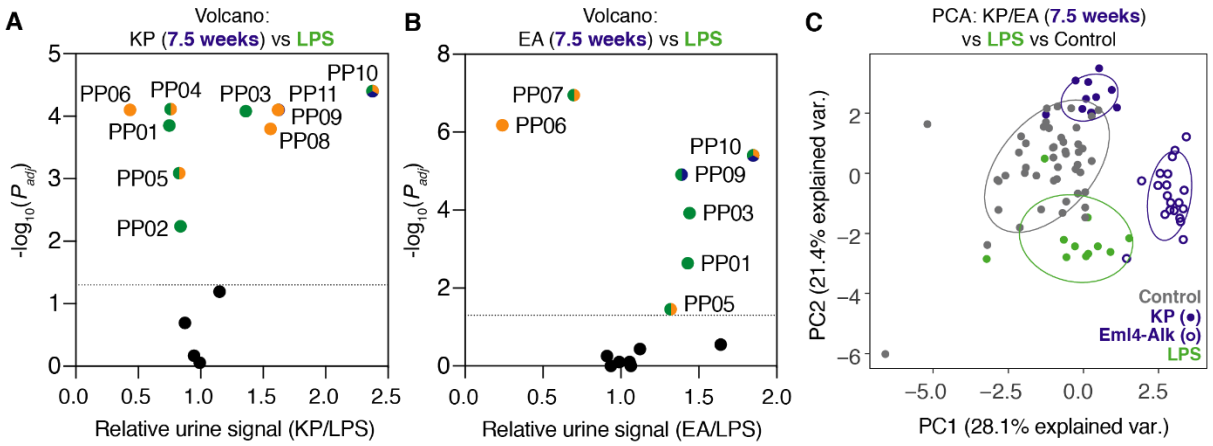

Fig. S13. Pulmonary activity-based nanosensor cleavage profile is distinct in lung cancer and benign lung inflammation. (**A-B**) Volcano plots of urinary reporter outputs from $KP_{7.5wk}$ (n = 11) (A) and $EA_{7.5wk}$ (n = 20) (B) mice relative to LPS-treated mice (n = 11), where $-\log_{10}(P_{adj})$ was plotted against fold change. Significance was calculated by two-tailed t-test with Holm-Sidak correction (for normally distributed reporters) or Mann-Whitney test with Bonferroni correction [for PP06, PP08, PP09, PP10, and PP11 in (A); PP06, PP08, PP10, PP11, and PP14 in (B)]. Dotted line is at P_{adj} = 0.05. Significant reporters are color-coded according to the classes of protease that cleave their corresponding peptide substrates *in vitro* (fig. S4) (green, metalloprotease-specific; orange, serine protease-specific; blue, aspartic protease-specific). (**C**) PCA of urinary reporter outputs from $KP_{7.5wk}$ (n = 11), $EA_{7.5wk}$ (n = 20), and LPS (n = 11) mice, as well as healthy control mice from all three experiments (n = 47).

Table S1. Reporter and substrate sequences for in vitro recombinant protease screen. 5FAM, 5-Carboxyfluorescein; CPQ2, quencher; PEG, polyethylene glycol; Cha, 3-Cyclohexylalanine; Cys(Me), methyl-cysteine; lowercase letters, *D*-amino acids.

Name	Fluorophore	Substrate
PPQ1	5FAM	GGPQGIWGQK(CPQ2)-PEG2-C
PPQ2	5FAM	GGPVGLIGK(CPQ2)-PEG2-C
PPQ3	5FAM	GGPVPLSLVMK(CPQ2)-PEG2-C
PPQ4	5FAM	GGPLGLRSWK(CPQ2)-PEG2-C
PPQ5	5FAM	GGPLGVRGKK(CPQ2)-PEG2-C
PPQ6	5FAM	GGfPRSGGGK(CPQ2)-PEG2-C
PPQ7	5FAM	GGLGPKGQTGK(CPQ2)-kk-PEG2-C
PPQ8	5FAM	GGGSGRSANAKG-K(CPQ2)-PEG2-GC
PPQ9	5FAM	GKPISLISSG-K(CPQ2)-PEG2-GC
PPQ10	5FAM	GILSRIVGGG-K(CPQ2)-PEG2-GC
PPQ11	5FAM	GSGSKIIGGG-K(CPQ2)-PEG2-GC
PPQ12	5FAM	GGPLGMRGG-K(CPQ2)-GC
PPQ13	5FAM	GP-(Cha)-G-Cys(Me)-HAG-K(CPQ2)-GC
PPQ14	5FAM	GAPFEMSAG-K(CPQ2)-GC

Table S2. Quantification of tumor burden in KP mice by microCT. V_{avg}, average tumor volume. MicroCT sensitivity is defined as the number of mice with detectable tumors divided by the total number of mice at each time point.

	5 weeks		7.5 weeks		10.5 weeks	
Mouse	**Multiplicity**	**Volume (mm^3)**	**Multiplicity**	**Volume (mm^3)**	**Multiplicity**	**Volume (mm^3)**
KP1	0	0	1	0.5	1	0.5
KP2	0	0	0	0	3	5.2
KP3	1	1.8	3	2.8	6	13
KP4	3	2.8	3	6.5	6	27
KP5	0	0	0	0	5	17.8
KP6	0	0	6	4.4	6	22.7
KP7	2	4.7	4	7	4	16.8
KP8	0	0	2	1	Motion Artifact	Motion Artifact
KP9	0	0	2	4.7	3	42.6
KP10	0	0	0	0	3	16.8
KP11	0	0	2	4.7	2	4.7
KP12	1	0.5	1	1.8	8	43.9
MicroCT Sensitivity	**33.3%**		**75%**		**100%**	
V_{avg} (mm^3)	**0.775**		**2.78**		**19.2**	

Table S3. Composition of training and test cohorts for random forest classification. Cohort numbers used to train and test random forest classifiers applied in Fig. 6A-C (KP v. Healthy, Eml4-Alk v. Healthy, LUAD v. Healthy) and Fig. 6D (LUAD v. Benign).

	5 weeks		7.5 weeks		10.5 weeks	
KP v. Healthy (Fig. 6A)	**Train**	**Test**	**Train**	**Test**	**Train**	**Test**
Healthy	0	9	12	6	0	12
KP	0	11	6	5	0	12
Eml4-Alk	0	0	6	0	0	0
Eml4-Alk v. Healthy (Fig. 6B)	**Train**	**Test**	**Train**	**Test**	**Train**	**Test**
Healthy	0	17	12	13	0	19
KP	0	0	6	0	0	0
Eml4-Alk	0	19	6	14	0	16
LUAD v. Healthy (Fig. 6C)	**Train**	**Test**	**Train**	**Test**	**Train**	**Test**
Healthy	0	26	12	19	0	31
KP	0	11	6	5	0	12
Eml4-Alk	0	19	6	14	0	16
LUAD v. Benign (Fig. 6D)	**Train**	**Test**	**Train**	**Test**	**Train**	**Test**
Healthy	0	0	12	19	0	0
KP	0	0	6	5	0	0
Eml4-Alk	0	0	6	14	0	0
LPS	0	0	6	5	0	0

Data file S1. Raw data from figures. Available separately as an Excel file.